Open Ceramics 5 (2021) 100048

Contents lists available at ScienceDirect

Open Ceramics

journal homepage: www.editorialmanager.com/oceram

CO_2 adsorption at intermediate and low temperature by geopolymer-hydrotalcite composites

E. Papa [a], E. Landi [a], A. Natali Murri [a], F. Miccio [a], A. Vaccari [a,b], V. Medri [a,*]

[a] ISTEC-CNR, Institute of Science and Technology for Ceramics, 48018, Faenza, Ravenna, Italy
[b] "Toso Montanari" Department of Industrial Chemistry, University of Bologna, 40100, Bologna, Italy

ARTICLE INFO

Keywords:
Geopolymer
Hydrotalcite
CO_2 adsorption
Composite
Physisorption
Chemisorption

ABSTRACT

Geopolymer-hydrotalcites composites have been prepared and compared to explore their use in the field of CO_2 adsorption for a wide range of working temperatures and relative applications. Two commercial hydrotalcites, with different Mg:Al ratio, were tested as fillers for a geopolymer matrix up to the maximum of 37 wt%. A high compressive strength (25–27 MPa) was retained in composites at 500 °C, which is the temperature of hydrotalcites transformation into amorphous mixed solid oxides able to adsorb CO_2. Composites were characterized in term of working capacity by testing the CO_2 adsorption at low (35 °C) and intermediate (200 °C) temperature, with cycles of adsorption/desorption and regeneration at 500 °C. At 35 °C, CO_2 physisorption capacity was between 0.079 and 0.154 mmol g^{-1}, while at 200 °C, the total CO_2 capacity value was between 0.114 and 0.141 mmol g^{-1}.

1. Introduction

In recent years, the sequestration of CO_2 downstream of industrial processes has been the subject of in-depth investigations [1]. The adsorption of CO_2 is also of great importance for the direct use of biogas [2] where the methane must be purified before being introduced into the distribution network, as a renewable alternative to natural gas.

The choice of the separation technology depends on the impact of the industrial process, on the efficiency of the adsorbent and on economic factors. Physical adsorption is a less-energy-intensive separation technology resulting an economic alternative in comparison to others [3]. In most cases, the solid adsorbents are in the form of monoliths or granules to facilitate handling and storage [4]. The adsorbent material must have high resistance to abrasion and withstand rapid changes in temperature and/or pressure, as the methods of regenerating the adsorbent with the release of CO_2 require fluctuations in pressure and/or temperature [5,6]. The key parameter for assessing the validity of an adsorbent is the specific adsorption capacity of CO_2 (moles of CO_2 per kg of material), which depends on the molecular structure, the morphology of the material, the temperature and the pressure. The ease of regeneration is another important parameter, since in the industrial field it is essential that regeneration is simple and inexpensive in order not to significantly affect the cost of the process.

Zeolites [7], activated carbon [8] and Metal Organic Frameworks (MOF) [9] are the most commonly used adsorbents. Geopolymers have been recently considered as adsorbents for CO_2 [10] at low temperature since they are similar to zeolites but less expensive [11]. They have a high selectivity in the adsorption of CO_2 [12], good mechanical properties and are easily formable in structures suitable for end use [13]. Previous studies reported that geopolymers can selectively adsorb CO_2 with an appreciable adsorption capacity in the range 0.27–0.29 mmol g^{-1} [12]. By introducing zeolites in the composition, CO_2 adsorption values increased up to 1.1 mmol g^{-1} at 0.1 bar of CO_2 at 35 °C [14,15].

Anionic clays such as hydrotalcites are layered double hydroxides (LDH), with the final general formula $[M^{2+}_{1-x}\ M^{3+}_{x}\ (OH)_2]^{x+}\ [A^{n-}]_{x/n} \cdot mH_2O$ (where M = metal and A = anion, usually carbonate) [6,16], and they are known both as adsorbents and as catalysts or heterogeneous supports [17,18]. Furthermore, the thermal evolution of hydrotalcites, with formation of a mixed oxide material with high surface area and good stability at high temperature, is crucial to enhance their CO_2 adsorption capacity [19]. Hydrotalcites present deficiencies related to shaping, stability and mechanical strength, which could be overcome by the presence of a suitable binding matrix such as geopolymers. In light of this, in a previous work, the authors have conceived new composites mixing a geopolymer matrix with hydrotalcites, having different Mg:Al molar ratios, in order to expand the use of these materials to a wider

* Corresponding author.
E-mail address: valentina.medri@istec.cnr.it (V. Medri).

https://doi.org/10.1016/j.oceram.2020.100048
Received 13 November 2020; Received in revised form 11 December 2020; Accepted 14 December 2020
Available online 16 December 2020

range of applications in the field of CO_2 adsorption, even at intermediate temperatures [20]. After a calcination at 500 °C, the adsorption capacity at 200 °C of composites with 28 wt% hydrotalcites was in the range 0.109–0.145 mmol g^{-1}, up to 30% less of the attended values, indicating a partial deactivation of hydrotalcites [20].

Therefore, by making composites with a higher amount of hydrotalcite (up to 37 wt%), the aim of this work is to enhance the adsorption capacity combining the properties of the two components for the production of a promising CO_2 sorbent, active at low (35 °C) and intermediate (200 °C) temperatures.

The composites were characterized and especially tested for CO_2 adsorption at different temperatures performing ad(de)sorption cycles. With the proper understanding of composition-structure-property relationships, composites may, conceivably, be synthesized and tailored as effective sorbents for CO_2 separation and capture to be applied in an extended temperature range.

2. Materials and methods

2.1. Samples preparation

Two commercial hydrotalcites (basic magnesium aluminum hydroxy carbonate powder) Pural®50 and Pural®70 by Sasol (D), coded as P50 and P70, respectively, were used as fillers. Hydrotalcites were deeply characterized in a previous paper [20]. Table 1 reports the main physiochemical properties of the powders before and after the thermal treatment at 500 °C for 5 h. The thermal treatment was selected after previous characterization [20] in order to turn hydrotalcites into amorphous Mg:Al mixed solid oxides, more performing for CO_2 adsorption [19].

The composite samples were obtained mixing the commercial hydrotalcites with a geopolymer matrix (coded G) with a Si:Al molar ratio equal to 2.0. The hydrotalcite content was maximized limiting as much as possible the additional water amount needed to maintain a plastic consistency of the mixture, while avoiding a remarkable loss of mechanical properties in the consolidated composites. The geopolymer slurry was first prepared mixing metakaolin (grade M1200S, purchased from Imerys; Ssa = 25 $m^2 g^{-1}$, d_{50} = 1.5 mm) with a potassium di-silicate aqueous solution (molar ratios H_2O:K_2O = 13.5 and SiO_2:K_2O = 2.0). The geopolymer slurry was obtained using a planetary centrifugal mixer (Thinky Mixer ARE-500, by Thinky, Japan). Hydrotalcite and water were then added to the geopolymer slurry, in the quantity reported in Table 2, and mixed and de-foamed with the centrifugal mixer.

Samples were cast in plastic molds and cured at 80 °C for ≈24 h, obtaining cylindrical specimens (Ø = 17 mm, h = 27 mm). The specimens were pulverized and, if necessary, calcined at 500 °C for 5 h for the subsequent characterization. The composites are coded as GPx, where Px indicate the hydrotalcite type (see Table 2).

2.2. Characterization techniques

The morphological and microstructural features were examined on gold-coated powder samples by a field emission gun-scanning electron microscope (FE-SEM, ΣIGMA: Zeiss, Germany). The real density was measured on powder samples using a helium pycnometer (Multivolume pycnometer 1305 by Micrometrics), while the bulk density was determined by weight-to-volume ratio, geometrically measuring with a caliper the volume of cylindrical specimens.

Table 1
Physiochemical properties of hydrotalcites before and after calcination at 500 °C for 5 h [20].

Hydrotalcite	Mg:Al	True density (g cm^{-3})		Ssa ($m^2 g^{-1}$)	
		As received	Calcined	As received	Calcined
P50	1.4	2.09	2.88	10	126
P70	3.1	2.10	2.98	17	101

Table 2
Composites coding and formulation.

Composite	Hydrotalcite		Water wt.%
	type	wt.%	
GP50	Pural 50	37	1
GP70	Pural 70	35	1

Attenuated Total Reflection (ATR) measurements were recorded using a Thermo Scientific Nicolet iS5 FTIR Spectrometer equipped with iD7 ATR accessory and diamond crystal. Each spectrum in the 4000-400 cm^{-1} range was obtained from the sum of 32 individual measurements recorded in order to minimize the noise signal.

A mercury intrusion porosimeter (MIP, surface tension = 0.48 N/m and contact angle = 140°, Thermo Finnigan Pascal 140 and Thermo Finnigan Pascal 240) was used to analyze the pore size distribution of the bulk materials, in the range 0.0058–100 μm.

The measurements of specific surface area were conducted on powder samples using a Thermo ScientificTM Surfer instrument and the specific surface area (Ssa) was calculated by the Brunauer–Emmet–Teller (BET) method by means of nitrogen adsorption at 77 K.

Cylindrical specimens (Ø = 17 mm, h = 27 mm) were used to test compressive strength at room temperature (test performed on 4 specimens) and at 500 °C (test performed on 3 specimens) by means of a universal testing machine (Zwick Z050, loading cell class 05, GmbH, Ulm, Germany) with a cross-head speed of 2 mm min^{-1}. A $MoSi_2$ element furnace (MDS66C, Instron SFL, Thornbury, Bristol, UK) was used for tests in temperature: samples were kept for 1 h at 500 °C before performing the test.

Intermediate (200 °C) and low temperature (35 °C) CO_2 sorption measurements were carried out flowing a dry mixture gas, composed of 50% CO_2 in Ar, on powders (pretreated for 5 h at 500 °C) of pure hydrotalcites and composites, using a thermogravimetric method (Netzsch STA449 Jupiter instrument). Concerning the intermediate temperature, the loaded powders were first heated at 500 °C for 1 h, then cooled down to 200 °C and kept at the selected temperature for 30 min under a pure argon gas flux (40 ml min^{-1}) before flowing CO_2 (40 ml min^{-1}) for 20 min. The total CO_2 working capacity (ΔW/Wo %), was determined from the difference in the material weight under these conditions and the corresponding CO_2 amount, in terms of mmol per gram of material, was calculated. The first CO_2 sorption was measured as combined or total sorption. Physisorption (namely reversible CO_2 sorption) and chemisorption (irreversible CO_2 sorption) were determined by a subsequent heat treatment at 200 °C for 20 min with a pure Ar gas flux, where the occurred weight loss referred to physisorption. Samples were then regenerated by heat treatment at 500 °C for 1 h under an Ar flux.

These conditions were used to operate two consecutive cycles of ad(de)sorption and regeneration or to verify the reproducibility of the samples over five cycles of ad(de)sorption.

The CO_2 working capacity of the materials was also studied at low temperature, namely 35 °C, performing five consecutive cycles of ad(de)sorption after the conditioning step at 500 °C.

X-ray diffraction (XRD) patterns were collected on powdered samples before and after thermal treatment at 500 °C and CO_2 adsorption at 200 °C (Powder Diffractometer Bruker D8 Advance with CuKα radiation, D).

3. Results and discussion

3.1. Microstructural characterization

The microstructure of the composites before and after the treatments at 500 °C is showed in Fig. 1.

In general, nanoprecipitates and mesopores typical of the geopolymer matrix are evident, together with the hydrotalcite structures, preserved also after the thermal treatment (Fig. 1b,d). As already reported [20],

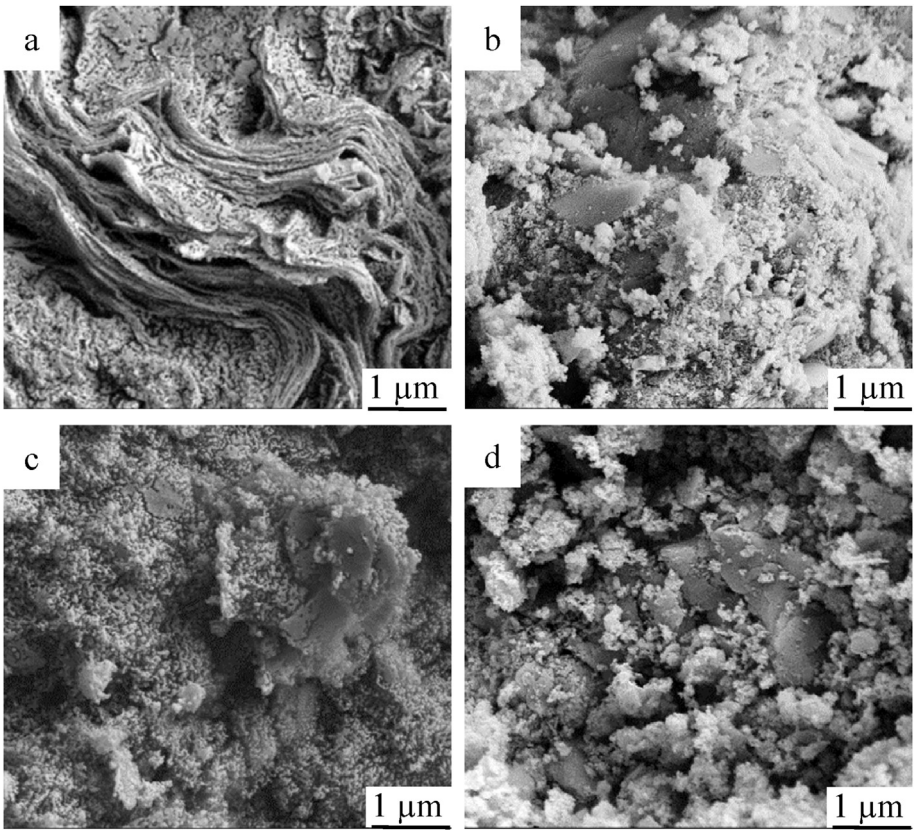

Fig. 1. SEM micrographs of GP50 dried (a) and calcined (b) and of GP70 dried (c) and calcined (d).

hydrotalcites P50 and P70 show spherical shaped particles. In particular, P50 has a coral-like structure formed by layers, well evident in Fig. 1a, while P70 presents shell-like particles with big holes [20]. The characteristic P70 particles shape allows the incorporation of the geopolymer matrix within the structure (Fig. 1c). Shrinkages and weight losses after the treatment at 500 °C and true (pycnometric) and bulk (geometrical) densities of untreated and thermally treated samples are reported in Table 3. The transformation of hydrotalcites into more compact oxide structures after the thermal treatment is responsible for the increase of the true density, as well for the decrease of bulk density, and for the evidences of shrinkages and weight losses (due to water removal, dehydroxylation and the elimination of CO_2 from HT interlayers [20, 21]).

3.2. ATR-FTIR characterization

The ATR-FTIR spectra of the dried composites and the as received hydrotalcites used as additive are reported in Fig. 2a, while Fig. 2b reports the spectra of composites and hydrotalcites after calcination.

The characteristic vibrations of hydrotalcites can be approximately associated to those of the constituent units, i.e., the interlayer anions, the hydroxyl groups (molecular vibrations) and the octahedral layers (lattice vibrations) [22]. The layered hydroxide nature of these compounds is well visible in the hydrogen vibrations identified around 3400-3600 cm^{-1} (stretching) (Fig. 2a) [22]. Furthermore, the stretching mode falls at higher vibrational frequencies with increasing the Mg:Al ratio in the hydrotalcites (Table 1), which is due to the decrease in layer spacing with increasing the aluminum substitution [22]. The presence of carbonate in the interlayer is indicated by the band at 1360 cm^{-1}, corresponding to the most sensitive carbonate vibration (ν_3 vibrational mode) [22]. Broad bands at around 554 cm^{-1}, 788 cm^{-1} and 947 cm^{-1} can be attributed to Al–O stretching modes [19]. As mentioned before [20], structural changes by dehydroxilation and decarbonation at higher temperature changed the interlayer distance in the hydrotalcites. With the removal of interlayer water upon heating, the intensity of the hydroxyl-stretching band at around 3400 cm^{-1} and the signal at 1640 cm^{-1} decreases accordingly (Fig. 2b). In addition, there is a decrease of the Al-related vibrations at 554, 788 and 947 cm^{-1}, which become broad and difficult to identify. Moreover, changes in carbonate vibrations are observed with a decrease of the intensity of peak at 1360 cm^{-1}.

The ATR-FTIR spectra of the composites evidence the coexistence of the geopolymer matrix and hydrotalcites and the thermal evolution of the latter. Indeed, Fig. 2a and b shows the same peaks trends observed before for hydrotalcites, plus the peaks characteristic of the geopolymer matrix. In detail, the broad band at 3400 cm^{-1} and the peak at 1640 cm^{-1} are due to OH stretching and bending vibration of H_2O respectively, while the most intense peak, centered at 980 cm^{-1}, is due to the Si–O–Si, Si–O–Al stretching. The thermal treatment at 500 °C suppressed the

Table 3
True and bulk densities of untreated and thermally treated samples and linear shrinkages (ΔΦ, diameter, and ΔH, height) and weight losses (ΔW) after the treatment at 500 °C.

Composite	True density (g cm^{-3})		Bulk density (g cm^{-3})		ΔH (%)	ΔØ (%)	ΔW (%)
	Dried	Calcined	Dried	Calcined	Calcined	Calcined	Calcined
GP50	2.21	2.50	1.37	1.30	−5.5	−5.5	−21
GP70	2.20	2.46	1.34	1.17	−3.9	−3.2	−21

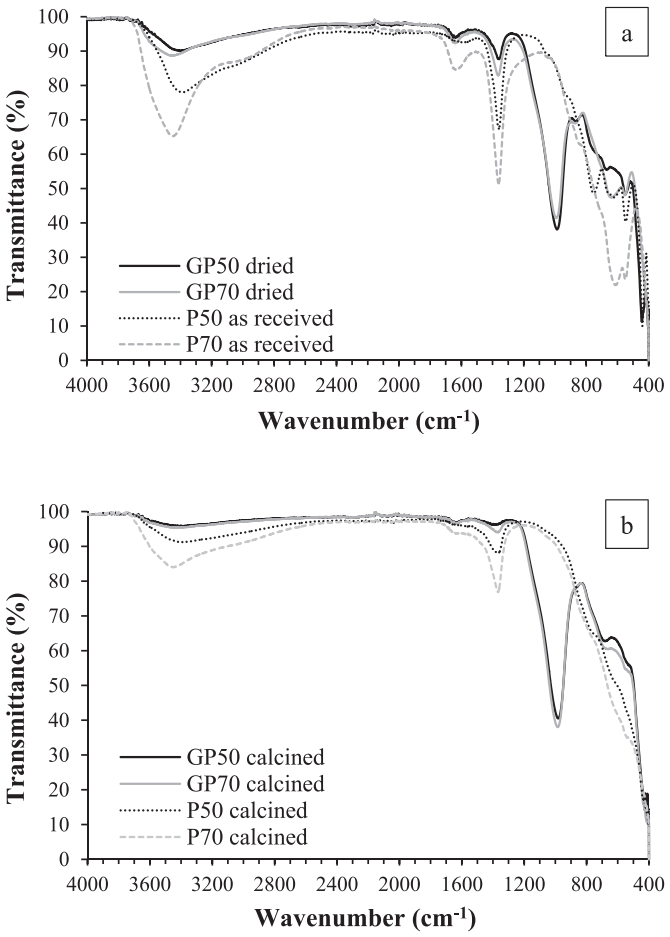

Fig. 2. ATR-FTIR spectra of dried samples GP50, GP70 and hydrotalcites P50 and P70 (a) and of the same after calcination (b).

hydrotalcite peaks, leaving unchanged the peaks identifying the geopolymer matrix.

3.3. Porosity and specific surface area

Pore size distributions of the bulk composites before and after calcination were obtained in the range 0.007–100 μm through MIP analysis and showed in Fig. 3, while in Table 4 the main results of total porosity %, total mercury intruded volume and modal pore diameter are resumed.

All samples show a prevalent monomodal distribution centered at 0.01 μm for GP50 and 0.03 μm for GP70. GP70 shows a more expanded pore size distribution in the range 0.007–0.050 μm. In general, an increase of few % of total porosity is detected after calcination, probably due to the transformation of the hydrotalcite (decarbonation) and complete water removal, while no significant changes in the pore size distribution are observed.

Concerning the specific surface area, values remain substantially unchanged after the heat treatment (Table 4) with a higher surface area for GP50. This is probably due to both a greater increase of the specific surface area of P50 after the thermal treatment (Table 1), both to the shell-like morphology of P70 observed in Refs. [20]. This likely favored the incorporation of the hydrotalcite in the geopolymer matrix compacting the structure and decreasing the surface area.

3.4. Mechanical characterization

Compressive strength tests performed at room temperature and at 500 °C show stress-strain curves with a jagged behavior, as shown in Fig. 4 as example. This is typical of porous samples where the rupture does not occur in a catastrophic way, but progressively involving the composite's struts.

In general, during the shaping of the specimens some air-bubbles might have been trapped inside the material; the struts surrounding those macropores firstly start to show failure under compressive loading, then the cracks propagate and accumulate until reaching the maximum stress, resulting in the final collapse of the whole sample. In the case of GP50 at room temperature, the coral like structure of the hydrotalcite is responsible of both a pronounced jagged behavior, because the rupture progressively involves the bridges among the layers and voids, both a high standard deviation, since P50 particles act as critical defects under compression, being not homogenously incorporated into the geopolymer matrix.

The average strength values obtained for the composites at r.t. and 500 °C are comparable and around 26 MPa. As a general result, the treatment at 500 °C adopted to activate the structure of the hydrotalcites does not cause any negative effect on the mechanical resistance of the materials. Indeed, hydrotalcites transform into more compact mixed oxides (MgO-like or Mg(Al)O oxides) through phenomena as water dehydration, dehydroxylation of layered OH groups and release of interlayer CO_3^{2-} [20,21]. The formation of such more compact oxides is probably responsible for the lowering of the standard deviation value obtained for the compressive strength, especially for GP50 (Table 5).

3.5. CO_2 adsorption capacity

The working capacity and reversible CO_2 ad(de)sorption properties of the composites were tested at intermediate (200 °C) and low temperature (35 °C). Fig. 5 shows the test at 200 °C with two consecutive cycles of CO_2 ad(de)sorption and regeneration. Physical adsorption involves interaction of CO_2 with basic sites in the hydrotalcite, while the irreversible chemisorption is due to carbonation/mineralization of the Mg^{2+} cations [23]. Indeed, as observed in X-ray diffraction patterns of GP50 (Fig. 6), the basal reflections of the (003), (006), (009), (110) and (113) planes typical of Mg–Al–CO_3 hydrotalcites [17,24] disappear after thermal treatment at 500 °C, while a broad reflection appears at about $2\theta = 43°$, due to the formation of MgO-type mixed oxide [20]. After CO_2 adsorption at 200 °C, the CO_2 chemisorption is confirmed as the main peaks of the Mg–Al–CO_3 material reappear, albeit with reduced intensity, in the XRD pattern. Conversely, the geopolymer matrix remain unchanged, also after the thermal treatment, showing the typical amorphous hump at about $2\theta = 27°$ and peaks due to unreacted crystalline impurities present in the starting metakaolin.

During the isothermal step at 200 °C, the desorption that occurs under the gas stream of pure Ar is due to the removal of the physisorbed CO_2 [20]. The chemisorbed CO_2 can be removed only when the step temperature increases at 500 °C, with consequent regeneration of the starting material and its whole working capacity.

The CO_2 adsorption at 200 °C for P50 and P70 is a combination of physical and chemical interactions [20]. A 1:1 contribution for the physisorption and chemisorption is assessed for the composites GP50 and GP70, as previously observed for samples containing the 28 wt% of hydrotalcites [20]. A partial decrease of the CO_2 working capacity is seen in the second cycle, which is expressed as CO_2% decay in Table 6.

Focusing on the 2nd cycle at 200 °C (Table 6), increasing the amount of P50 in the composite from 28 wt% [20] to 37 wt% gives a 28% improvement in the sorption capacity of the material (from 0.089 to 0.114 mmol g^{-1}), while the CO_2% adsorption decay is nearly unchanged (18% and 19%, respectively). Interestingly when the P70 amount is increased from 28 wt% to 35 wt%, the capacity improves by only 8% (from 0.091 to 0.098 mmol g^{-1}), while the lowest decay (14%) is obtained for GP70, which is significantly different from that (20%) of the composite with a lower amount of P70.

The performance of the materials after the calcination at 500 °C was also tested under five consecutive cycles of ad(de)sorption at 200 °C, to

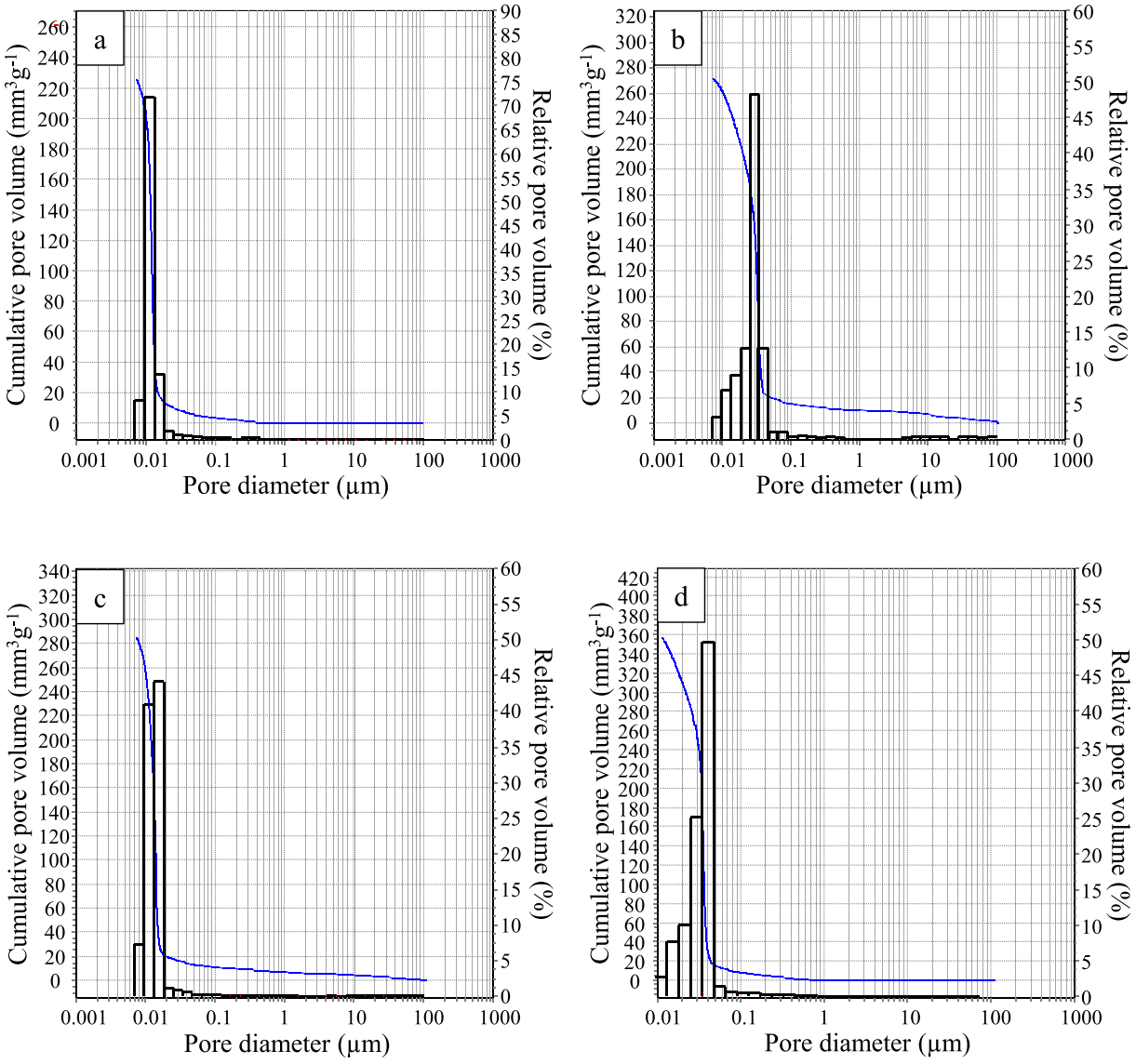

Fig. 3. Pore size distribution by Hg intrusion porosimetry (MIP) of sample GP50 dried (a) and calcined (c) and of sample GP70 dried (b) and calcined (d).

Table 4
Total open porosity, total mercury intruded volume, modal pore diameter obtained by MIP and BET Specific surface area for samples GP50 and GP70 dried and after calcination.

Composite	Porosity by MIP (%)		Tot V ($mm^3\ g^{-1}$)		Modal Ø (µm)		Ssa ($m^2\ g^{-1}$)	
	Dried	Calcined	Dried	Calcined	Dried	Calcined	Dried	Calcined
GP50	33	37	226	285	0.01	0.01	56	52
GP70	36	43	271	357	0.03	0.03	33	32

assess if ageing phenomena might affect the physisorption capacity. GP50 composite shows the lowest capacity loss (13%) moving from the first to the fifth step compared to both pure hydrotalcites and GP70 (capacity loss >20%). For GP50 a limited decrease in physisorption is detected from the first (0.070 mmol g^{-1}) toward the fifth cycle (0.061 mmol g^{-1}). In addition, the material after the regeneration at 500 °C shows again both the physical and chemical contributions at 200 °C and surprisingly without any detectable loss of performance. Contrarily, GP70 represents the worst case with a decay of about 36%, being the physisorption value for the first and the fifth cycle respectively 0.064 mmol g^{-1} and 0.041 mmol g^{-1}.

Since a good physical contribution (around 50%) is detected for composites at 200 °C, these materials have been supposed to be of interest at low temperature for pressure swing adsorption applications [19].

For this purpose, the CO_2 adsorption at 35 °C was preliminarily assessed by thermogravimetry on GP50 and GP70 composites, P50 and P70 hydrotalcites and the geopolymer matrix. Five consecutive cycles of ad(de)sorption were performed as showed in Fig. 7.

In general, the CO_2 adsorption is higher at 35 °C than 200 °C for all samples and at each cycle. Better material performances are expected at 35 °C compared to 200 °C, being physisorption favored as temperature

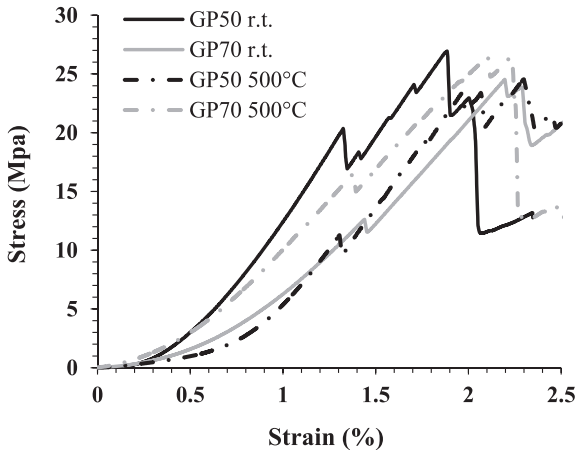

Fig. 4. Example of stress-strain curves for sample GP50 and for sample GP70 at r.t and 500 °C.

Table 5
Compressive strength at room temperature and 500 °C.

Composite	Compressive strength (MPa)	
	r.t.	500 °C
GP50	26 ± 7	25 ± 2
GP70	27 ± 5	27 ± 4

decreases. With increasing temperatures molecules have higher levels of kinetic energy and have a greater possibility to desorb from the surface, thus reducing the sorption values [19]. Indeed, the adsorption values at 200 °C, accounting for cumulative physisorption and chemisorption contributions, are about 30–40% of those detected at 35 °C for both the GP50 and GP70.

GP50 is the best performing composite at both 200 °C and 35 °C. The last cycles give good evidence of the reproducibility of the physical ad(de)sorption steps and can be referred as that of the material in 'stabilized conditions' for the two operating temperatures. Values calculated for the 5th cycle, entirely due to physical interactions of CO_2 with the material, are found to be equal to 0.061 mmol g^{-1} and 0.154 mmol g^{-1} at 200 °C and 35 °C respectively.

The 5th adsorption value obtained at 35 °C is of particular interest when compared to the expected value (0.112 mmol g^{-1}), calculated by the mixing rule (weighted contributions of the experimental adsorption of the matrix G and the pure hydrotalcite P50) (Fig. 8). GP50 composite shows a CO_2 physical adsorption at low temperature the 40% higher than that expected (Fig. 8). Conversely, GP70 is less performing than expected, showing an adsorption capacity of 0.079 mmol g^{-1} instead of 0.124 mmol g^{-1} (Fig. 8).

It is interesting to note that for GP50 the 5th physisorption at 35 °C (0.154 mmol g^{-1}) is even higher than the first whole (chemi- and physisorption) adsorption at 200 °C (0.141 mmol g^{-1}).

However, even if composites have the best performance at low temperatures, their chemical adsorption capacity allows them to be used even at high temperatures (where physisorption is limited), thus expanding the useful working temperature range [25]. At 200 °C, a regeneration step is obviously required before each cycle to exploit the chemisorption contribution of hydrotalcite.

4. Conclusion

Hydrotalcite-geopolymer composites were synthesized and studied for CO_2 adsorption at low (35 °C) and intermediate temperature (200 °C). Two commercial hydrotalcites (P50 and P70) with different Mg:Al ratio and morphology were tested as fillers for a geopolymer matrix, up to a maximum allowed of 37 wt%. Self-supporting, easily shapeable monoliths were obtained (GP50 and GP70), showing high mechanical strength (25–27 MPa) also at high temperature (500 °C). Such composites result suitable for applications where the adsorbent material must have high abrasion resistance and must withstand rapid changes in temperature and/or pressure conditions.

Regarding the CO_2 adsorption capacity, increasing the hydrotalcite

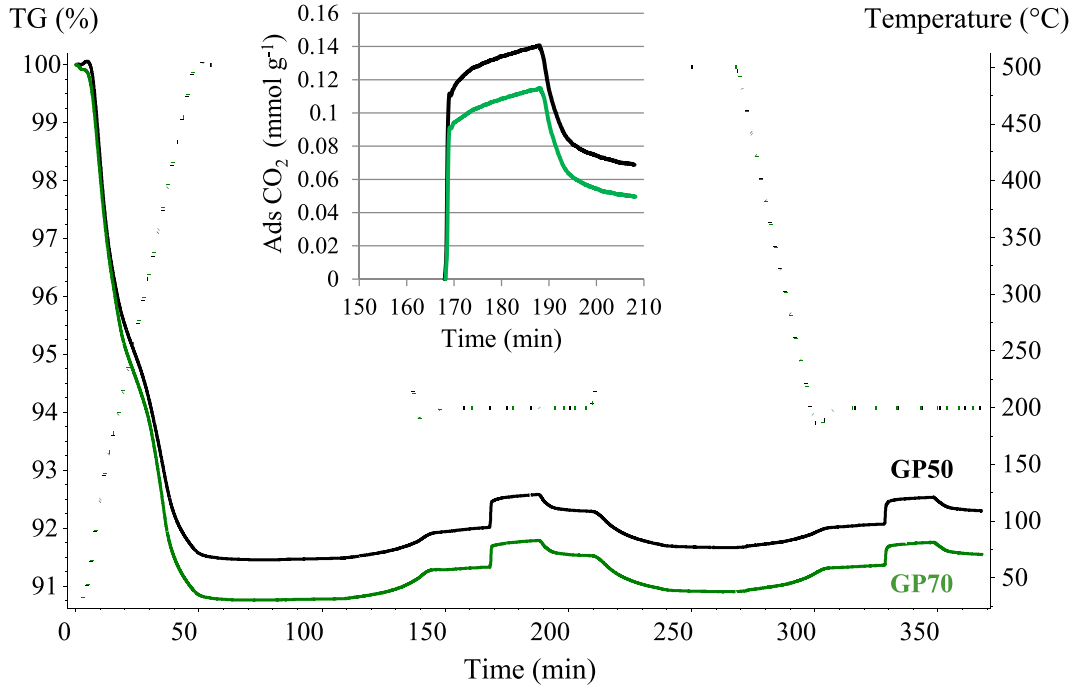

Fig. 5. TG analyses (solid line = TG curves, dotted line = temperature curves) of the composites GP50 and GP70. Two consecutive cycles of ad(de)sorption at 200 °C after treatment at 500 °C.

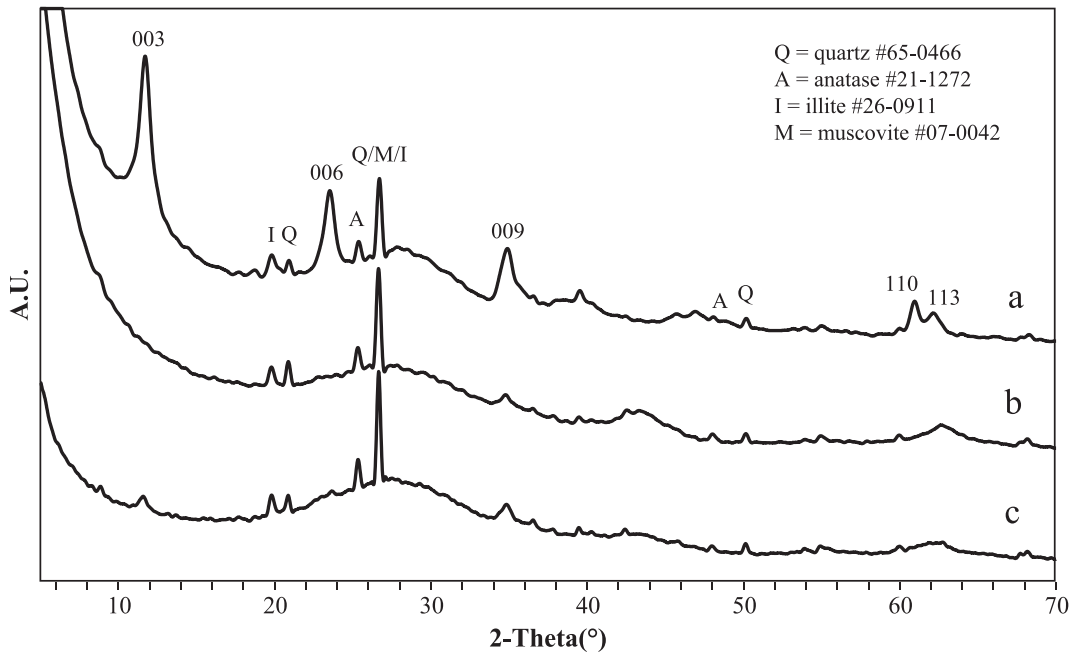

Fig. 6. XRD patterns of sample GP50 dried at 80 °C (a), calcined (b) and after CO_2 adsorption at 200 °C (c).

Table 6
CO_2 adsorption capacity, working capacity (ΔW/Wo), CO_2 physi- and chemi-adsorption, CO_2 decay % on two consecutive cycles of ad(de)sorption at 200 °C and regeneration at 500 °C.

Composite	1° cycle				2° cycle				CO_2 decay (%)
	CO_2 ads. (mmol g^{-1})	ΔW/Wo (%)	Physi ads. (%)	Chemi ads. (%)	CO_2 ads. (mmol g^{-1})	ΔW/Wo (%)	Physi ads. (%)	Chemi ads. (%)	
GP50	0.141	0.62	0.31	0.31	0.114	0.50	0.25	0.25	19
GP70	0.114	0.50	0.28	0.22	0.098	0.43	0.22	0.21	14
GHyT50 [20]	0.109	0.48	0.24	0.24	0.089	0.39	0.18	0.21	18
GHyT70 [20]	0.114	0.50	0.25	0.25	0.091	0.40	0.20	0.20	20

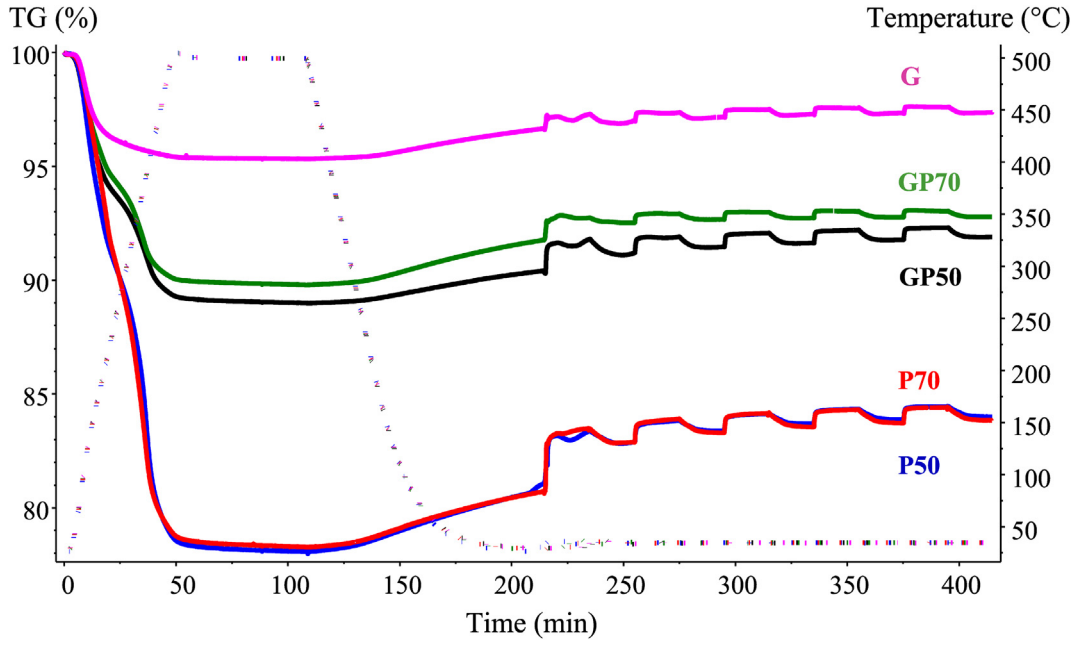

Fig. 7. TG analyses (solid line = TG curves, dotted line = temperature) for five consecutive cycles of ad(de)sorption at 35 °C performed on the composites GP50 and GP 70, the hydrotalcites P50 and P70 and the geopolymer matrix G.

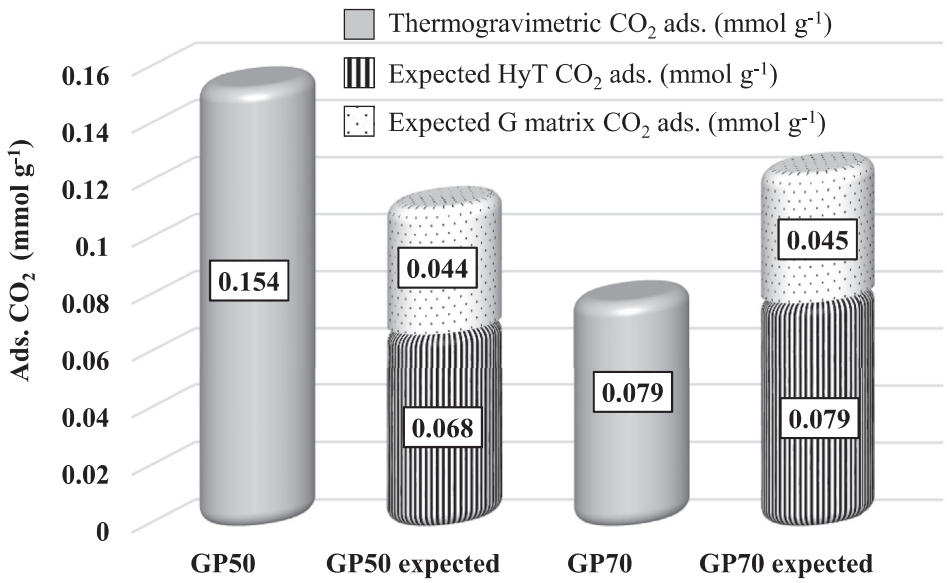

Fig. 8. CO_2 adsorption values (mmol g^{-1}) obtained by thermogravimetric analysis at 35 °C compared with the expected adsorption values calculated on the basis of the mixing rule i.e. sum of the relative wt.% contributions of the two components, hydrotalcite and geopolymer matrix.

amount from 28 wt% [20] to 37 wt% was beneficial in the case of P50. In fact, in the second adsorption cycle at 200 °C the CO_2 sorption capacity (0.141 mmol g^{-1}) of the material improved by the 28%.

In general, the CO_2 adsorption was higher at 35 °C than 200 °C for all the composites and GP50 was the best performing material. In particular, it showed a CO_2 physical adsorption at 35 °C (0.154 mmol g^{-1}) the 40% higher than that expected.

Due to the good physisorption performance at low temperature these materials could be employed for pressure swing adsorption applications. However, exploiting the chemisorption contribution of hydrotalcite at high temperature, where the physisorption is limited, these composites can be used in a wider range of working temperature.

Declaration of competing interest

The authors declare that they have no known competing financial interests or personal relationships that could have appeared to influence the work reported in this paper.

Acknowledgements

The authors greatly thank Mr. Davide De Pietri Tonelli for samples preparation and Mr. Cesare Melandri for mechanical tests.

References

[1] T. Kuramochi, A. Ramírez, W. Turkenburg, A. Faaij, Comparative assessment of CO_2 capture technologies for carbon-intensive industrial processes, Prog. Energy Combust. Sci. 38 (2012) 87–112.
[2] S. Chaemchuen, N. Alam Kabir, K. Zhou, F. Verpoort, Metal–organic frameworks for upgrading biogas via CO_2 adsorption to biogas green energy, Chem. Soc. Rev. 42 (2013) 9304–9332.
[3] S. Choi, J.H. Drese, C.W. Jones, Adsorbent materials for carbon dioxide capture from large anthropogenic point sources, ChemSusChem. 2 (2009) 796–854.
[4] F. Rezaei, P. Webley, Structured adsorbents in gas separation processes, Separ. Purif. Technol. 70 (2010) 243–256.
[5] Z. Yong, V. Mata, A.E. Rodrigues, Adsorption of carbon dioxide at high temperature—a review, Separ. Purif. Technol. 26 (2002) 195–205.
[6] Z. Yong, V. Mata, E. Rodrigues, Adsorption of carbon dioxide onto hydrotalcite-like compounds (HTlcs) at high temperatures, Ind. Eng. Chem. Res. 40 (2001) 204–209.
[7] Q. Wang, J. Luo, Z. Zhong, A. Borgna, CO_2 capture by solid adsorbents and their applications: current status and new trends, Energy Environ. Sci. 4 (2011) 42–55.
[8] A. Samanta, A. Zhao, G.K.H. Shimizu, P. Sarkar, R. Gupta, Post-combustion CO_2 capture using solid sorbents: a review, Ind. Eng. Chem. Res. 51 (2012) 1438–1463.
[9] F. Raganati, P. Ammendola, R. Chirone, CO_2 capture performances of fine solid sorbents in a sound-assisted fluidized bed, Powder Technol. 268 (2014) 347–356.
[10] R.M. Novais, R.C. Pullar, J.A. Labrincha, Geopolymer foams: an overview of recent advancements, Prog. Mater. Sci. 109 (2020) 100621.
[11] W.M. Kriven, J.L. Bell, M. Gordon, Microstructure and microchemistry of fully-reacted geopolymers and geopolymer matrix composites, Ceram. Trans. 153 (2013) 227–250.
[12] M. Minelli, V. Medri, E. Papa, F. Miccio, E. Landi, F. Doghieri, Geopolymers as solid adsorbent for CO2 capture, Chem. Eng. Sci. 148 (2016) 267–274.
[13] E. Landi, V. Medri, E. Papa, J. Dedecek, P. Klein, P. Benito, A. Vaccari, Alkali-bonded ceramics with hierarchical tailored porosity, Appl. Clay Sci. 73 (2013) 56–64.
[14] E. Papa, V. Medri, S. Amari, J. Manaud, P. Benito, A. Vaccari, E. Landi, Zeolite-geopolymer composite materials: production and characterization, J. Clean. Prod. 171 (2018) 76–84.
[15] M. Minelli, E. Papa, V. Medri, F. Miccio, P. Benito, F. Doghieri, E. Landi, Characterization of novel geopolymer – zeolite composites as solid adsorbents for CO_2 capture, Chem. Eng. J. 341 (2018) 505–515.
[16] O. Clause, M. Goncalves Coelho, M. Gazzano, D. Matteuzzi, F. Trifirò, A. Vaccari, Synthesis and thermal reactivity of nickel-containing anionic clays, Appl. Clay Sci. 8 (1993) 169–186.
[17] F. Cavani, F. Trifirò, A. Vaccari, Hydrotalcite-type anionic clays: preparation, properties and applications, Catal, Today Off. 11 (1991) 173–301.
[18] J.E. Olszówka, R. Karcz, E. Bielańska, J. Kryściak-Czerwenka, B.D. Napruszewska, B. Sulikowski, R.P. Socha, A. Gaweł, K. Bahranowski, Z. Olejniczak, E.M. Serwicka, New insight into the preferred valency of interlayer anions in hydrotalcite-like compounds: the effect of Mg/Al ratio, Appl. Clay Sci. 155 (2018) 84–94.
[19] M.K.R. Reddy, Z.P. Xu, G.Q. Lu, J.C.D. da Costa, Layered double hydroxides for CO_2 capture: structure evolution and regeneration, Ind. Eng. Chem. Res. 45 (2006) 7504–7509.
[20] E. Papa, V. Medri, C. Paillard, B. Contri, A. Natali Murri, A. Vaccari, E. Landi, Geopolymer-hydrotalcite composites for CO_2 capture, J. Clean. Prod. 237 (2019) 117738.
[21] T.S. Stanimirova, N. Piperov, N. Petrova, G. Kirov, Thermal evolution of Mg-Al-CO_3 hydrotalcites, Clay Miner. 39 (2004) 177–191.
[22] M.J. Hernandez-Moreno, M.A. Ulibarri, J.L. Rendon, C.J. Serna, IR characteristics of hydrotalcite-like compounds, Phys. Chem. Miner. 12 (1985) 34–38.
[23] N.D. Hutson, B.C. Attwood, High temperature adsorption of CO_2 on various hydrotalcite-like compounds, Adsorption 14 (2008) 781–789.
[24] Q. Wang, H.H. Tay, Z. Guo, L. Chen, Y. Liu, J. Chang, Z. Zhong, J. Luo, A. Borgna, Morphology and composition controllable synthesis of Mg-Al-CO_3 hydrotalcites by tuning the synthesis pH and the CO_2 capture capacity, Appl. Clay Sci. 55 (2012) 18–26.
[25] C. Megías-Sayago, R. Bingre, L. Huang, G. Lutzweiler, Q. Wang, B. Louis, CO_2 adsorption capacities in zeolites and layered double hydroxide materials, Front. Chem. 7 (2019) 551.